

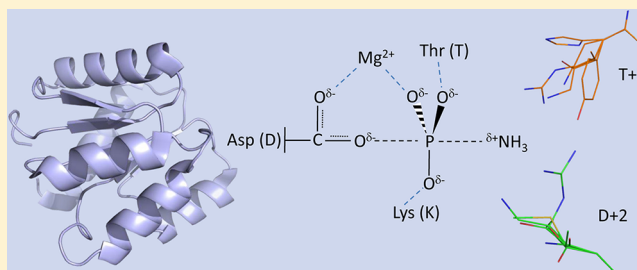
# Nonconserved Active Site Residues Modulate CheY Autophosphorylation Kinetics and Phosphodonor Preference

Stephanie A. Thomas, Robert M. Immormino, Robert B. Bourret, and Ruth E. Silversmith\*

Department of Microbiology and Immunology, University of North Carolina, Chapel Hill, North Carolina 27599-7290, United States

## S Supporting Information

**ABSTRACT:** In two-component signal transduction, response regulator proteins contain the catalytic machinery for their own covalent phosphorylation and can catalyze phosphotransfer from a partner sensor kinase or autophosphorylate using various small molecule phosphodonors. Although response regulator autophosphorylation is physiologically relevant and a powerful experimental tool, the kinetic determinants of the autophosphorylation reaction and how those determinants might vary for different response regulators and phosphodonors are largely unknown. We characterized the autophosphorylation kinetics of 21 variants of the model response regulator *Escherichia coli* CheY that contained substitutions primarily at nonconserved active site positions D + 2 (CheY residue 59) and T + 2 (CheY residue 89), two residues C-terminal to conserved D57 and T87, respectively. Overall, the CheY variants exhibited a  $>10^5$ -fold range of rate constants ( $k_{\text{phos}}/K_s$ ) for reaction with phosphoramidate, acetyl phosphate, or monophosphoimidazole, with the great majority of rates enhanced versus that of wild-type CheY. Although phosphodonor preference varied substantially, nearly all the CheY variants reacted faster with phosphoramidate than acetyl phosphate. Correlation between the increased positive charge of the D + 2 and T + 2 side chains and faster rates indicated electrostatic interactions are a kinetic determinant. Moreover, sensitivities of rate constants to ionic strength indicated that both long-range and localized electrostatic interactions influence autophosphorylation kinetics. The increased nonpolar surface area of the D + 2 and T + 2 side chains also correlated with an enhanced autophosphorylation rate, especially for reaction with phosphoramidate and monophosphoimidazole. Computer docking suggested that highly accelerated monophosphoimidazole autophosphorylation rates for CheY variants with a tyrosine at position T + 2 likely reflect structural mimicry of phosphotransfer from the sensor kinase histidyl phosphate.



Two-component signal transduction systems are ubiquitous in bacteria and control a variety of cellular processes.<sup>1–3</sup> Despite their amazing functional diversity, two-component systems share a fundamental signaling scheme based on the transfer of phosphoryl groups between conserved protein domains. Signal transduction involves autophosphorylation of a sensor kinase on a histidyl residue, typically modulated by environmental conditions. The phosphoryl group is then transferred to an aspartyl residue on a partner response regulator protein, which alters the ability of the response regulator to execute an output response. This central His to Asp phosphotransfer event is catalyzed by a conserved active site on the receiver domain of the response regulator. It has been recognized for more than 20 years that receiver domains can also catalyze their own phosphorylation using a variety of small molecule phosphodonors.<sup>4</sup> Response regulator autophosphorylation with the metabolic intermediate acetyl phosphate contributes to the regulation of multiple two-component systems in vivo,<sup>5,6</sup> and the use of small molecule phosphodonors in vitro has been instrumental in facilitating functional analysis of numerous response regulators.<sup>7–9</sup> Because autophosphorylation of the response regulator and phosphotransfer from the sensor kinase to the response regulator both proceed through the same basic phosphorus substitution chemistry,

mechanistic insights into the catalysis of response regulator autophosphorylation will enhance our understanding of the more complex phosphotransfer reaction between proteins.

Response regulator receiver domains have a conserved ( $\beta/\alpha$ )<sub>5</sub> fold with the conserved active site located on the  $\beta/\alpha$  loops that cluster on one face of the domain<sup>10</sup> (Figure 1A). The phosphorylatable aspartate (D) is positioned centrally in the active site and is surrounded by a threonine/serine (T), a lysine (K), and two additional acid residues (DD), which coordinate a magnesium ion. The Mg<sup>2+</sup>, threonine/serine, and lysine interact with the three phosphoryl oxygens in the phosphorylated forms of receivers.<sup>10,11</sup> On the basis of transition state analogue structures of related phosphatases within the haloacid dehalogenase superfamily,<sup>12</sup> the same interactions are also likely to occur in the response regulator transition state. Autophosphorylation proceeds by nucleophilic attack of the aspartyl carboxylate on the phosphodonor phosphorus atom in a substitution reaction. The receiver domain active site also

Received: December 12, 2012

Revised: March 4, 2013

Published: March 4, 2013



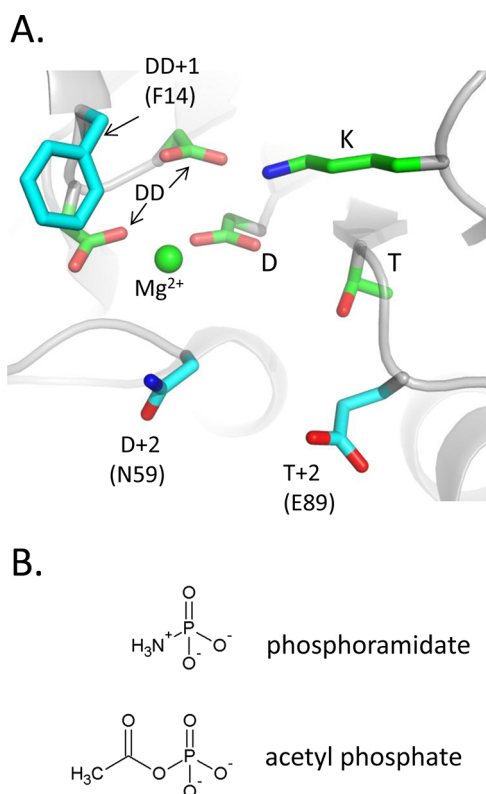


**Figure 1.** Features of the receiver domain active site (A) and chemical structures of phosphodonor molecules (B). (A) Active site of *Escherichia coli* CheY (Protein Data Bank entry 1FQW) with residues conserved among all receiver domains colored green and the three nonconserved residues studied here colored cyan. Conserved residues are labeled as outlined in the text: DD is the metal binding pair (CheY D12 and D13), D is the phosphorylated aspartate (CheY D57), and T and K are the conserved threonine/serine (CheY T87) and lysine, respectively (CheY K109). Nonconserved residues are labeled according to their sequence relationship to the closest conserved residue with their identities in *E. coli* CheY in parentheses. (B) Prototypes of the two chemical classes of phosphodonors. Phosphoramidate and acetyl phosphate represent the phosphoramidate and acyl phosphate chemical classes, respectively. Charges shown are predominant at pH 7.0. CheY reacts poorly with the unprotonated form of PAM ( $pK_a \sim 8.0$ ).<sup>18</sup>

catalyzes the subsequent hydrolysis of the aspartyl phosphate in a self-catalyzed dephosphorylation reaction.

Known small molecule phosphodonors for receiver domains fall into two chemical classes (Figure 1B). Phosphoramidates ( $R_2NH^+-PO_3^{2-}$ ) contain a phosphorus–nitrogen bond and include monophosphoimidazole (MPI), a near-identical model of the phosphohistidine side chain in sensor kinases. The class also includes the compound phosphoramidate (PAM,  $NH_3^+-PO_3^{2-}$ ), often used to phosphorylate response regulators *in vitro*, and the smallest compound in the class. The other phosphodonor class consists of acyl phosphates ( $RCO_2-PO_3^{2-}$ ), mixed anhydrides that include the physiologically relevant acetyl phosphate.<sup>6</sup> Both PAM and acetyl phosphate (AcP,  $CH_3CO_2-PO_3^{2-}$ ), well-characterized representatives of the two chemical classes, are relatively reactive to nucleophilic substitution. Both have high free energies of hydrolysis and undergo limited hydrolysis at neutral pH.<sup>13,14</sup> However, PAM and AcP differ in net charge, charge distribution, and size (Figure 1B).

Much of the kinetic and mechanistic characterization of receiver domain autophosphorylation has come from studies of the *Escherichia coli*/*Salmonella* chemotaxis response regulator CheY.<sup>15–18</sup> CheY consists only of a receiver domain and has a unique active site tryptophan residue that serves as a fluorescence probe for phosphorylation.<sup>4</sup> The rates of CheY autophosphorylation with PAM and AcP are similar<sup>16,18</sup> but much slower than the rate of phosphotransfer from the CheA kinase.<sup>19</sup> The disparity in rates of CheY phosphorylation appears to be partially due to weak binding between CheY and small molecule phosphodonors.<sup>15</sup> Plots of the pseudo-first-order autophosphorylation rate constant versus PAM or AcP concentration are linear up to at least 100 mM phosphodonor with no sign of saturation, indicating constants for binding between CheY and phosphodonor of  $\gg 100$  mM.<sup>15,17</sup> CheY does not use general acid catalysis in autophosphorylation with either PAM or AcP.<sup>18</sup> Although autophosphorylation kinetic data for other response regulators are limited, the available data suggest that different response regulators react with different kinetics<sup>20</sup> as well as preferences for different phosphodonors. For example, response regulators CheB<sup>+</sup> from *E. coli* and Spo0F<sup>21</sup> from *Bacillus subtilis* do not autophosphorylate with AcP but react readily with PAM. However, the structural features that determine the autophosphorylation kinetics of different receiver domains and how these features exert their modulatory effects are not currently known. *E. coli* CheY serves as a highly experimentally accessible model system for exploring features of receiver domains that modulate functional differences between response regulators, a family of signaling proteins with tens of thousands of known members.<sup>3,22</sup>

This study represents the first step toward a long-term goal of elucidating how various amino acids at nonconserved active site positions modulate the rates of response regulator autophosphorylation and phosphotransfer from the kinase. Examination of the active conformation of CheY [Protein Data Bank (PDB) entry 1FQW], believed to be the ground state for the autophosphorylation reaction,<sup>17,20,23</sup> reveals that nonconserved residues D + 2, T + 1, and T + 2 (CheY residues 59, 88, and 89, respectively; one or two residues C-terminal to the conserved D or T) form the surface of the active site where the phosphodonor molecule would be expected to approach and dock. In contrast, the conserved Asp, Thr/Ser, Lys, and divalent cation are located deeper within the CheY active site (Figure 1A). Thus, the conserved portions of the CheY active site are positioned to interact with the phosphoryl group of the phosphodonor, whereas the nonconserved portions are positioned to interact with the leaving group. In this work, we focus primarily on the effect of residues at positions D + 2 and T + 2 on autophosphorylation because response regulators exhibit far more amino acid sequence diversity at D + 2 and T + 2 than at T + 1, which is Ala or Gly in more than 70% of response regulators.<sup>22,24</sup> Furthermore, previous work from this laboratory examining the related self-catalyzed dephosphorylation reaction demonstrated that substitutions at positions D + 2 and T + 2 impact the rates of *E. coli* CheY and *B. subtilis* Spo0F autodephosphorylation and that a given residue often has similar effects on the reaction rates in the two response regulators.<sup>25,26</sup>

We show here that a set of 21 CheY mutants exhibited a  $>10^5$ -fold span of autophosphorylation rates with AcP, PAM, or MPI, with up to  $10^3$ -fold rate enhancements versus the rate of wild-type CheY. The great majority of the CheY variants reacted faster with PAM and MPI than with AcP. Statistical

correlations between autophosphorylation rates and side chain properties, aided by direct biochemical analysis and molecular modeling, allowed identification and characterization of several mechanisms for rate modulation and phosphodonor preference, including attractive electrostatic interactions and steric complementarity between CheY and the phosphodonor.

## ■ EXPERIMENTAL PROCEDURES

**Site-Directed Mutagenesis and Protein Purification.** Site-directed mutagenesis of the pRS3 plasmid,<sup>27</sup> which carries the *E. coli* *cheY* and *cheZ* genes under regulation of the *Serratia marcescens* *trp* promoter, was conducted using QuikChange methodology (Agilent Technologies). Resultant plasmids were transformed into *E. coli*  $\Delta$ *cheY* strain KO641*recA* for CheY expression and purification as described previously.<sup>26</sup>

**Chemicals.** Acetyl phosphate (AcP) (potassium lithium salt) was from Sigma-Aldrich. The potassium salt of phosphoramidate (PAM) was synthesized as described previously.<sup>28</sup> The PAM was >95% pure as assessed by <sup>31</sup>P NMR, with the remaining phosphorus present as inorganic phosphate. The calcium salt of monophosphoimidazole (MPI) was synthesized according to published protocols.<sup>29</sup> To prepare the sodium salt of MPI (Na<sub>2</sub>MPI), we passed an aqueous solution of CaMPI through a column containing Chelex resin in the sodium form (Bio-Rad) that had been washed in water, followed by flash freezing and lyophilization.

**Fluorescence Spectroscopy.** Time courses for reaction of CheY (wild type and mutant) with small molecule phosphodonors were measured by stopped-flow tryptophan fluorescence, essentially as described previously.<sup>17</sup> A rapid mixing device (Applied Photophysics RX2000) with a dead time of 8 ms was used to react equal volumes of solutions containing CheY and phosphodonor (AcP, PAM, or MPI) while maintaining a constant temperature of 25 ± 0.5 °C with a circulating water bath. Tryptophan fluorescence (excitation at 295 nm and emission at 346 nm) was recorded at 20 ms intervals using a Perkin-Elmer LS-50B luminescence spectrometer with FL Winlab version 1.1. The final reaction concentrations were 2.5 μM CheY and 0.5–30 mM phosphodonor. The CheY solutions were in 100 mM Hepes (pH 7.0) and 10 mM MgCl<sub>2</sub> (total ionic strength of 130 mM). The phosphodonor solutions were also in 100 mM Hepes (pH 7.0) and 10 mM MgCl<sub>2</sub> with appropriate amounts of KCl to maintain a constant ionic strength of 330 mM in spite of differing phosphodonor concentrations. Thus, mixing of equal volumes of the CheY and phosphodonor solutions yielded a final reaction ionic strength of 230 mM. A minimum of four phosphodonor concentrations were tested for each CheY variant, and a series of three to five time courses were recorded for each phosphodonor concentration. The range of phosphodonor concentrations was adjusted for each CheY variant to give *k*<sub>obs</sub> values between ~0.05 and 8 s<sup>-1</sup>. The entire process was conducted in duplicate for each CheY variant.

Reactions resulted in an exponential loss of tryptophan fluorescence because of the phosphorylation of CheY Asp57. The time courses were fit to an equation for a single-exponential decay using either Excel or Prism to obtain a pseudo-first-order rate constant (*k*<sub>obs</sub>) that reflects the rate of accumulation of phosphorylated CheY. Plots of *k*<sub>obs</sub> (averaged from three to five replicates) versus phosphodonor concentration were linear for all the CheY variants and phosphodonor concentrations used in this study, consistent with the previously derived relationship:<sup>15–17</sup>

$$k_{\text{obs}} = (k_{\text{phos}}/K_S)[\text{phosphodonor}] + k_{\text{dephos}} \quad (1)$$

where *K*<sub>S</sub> is the dissociation equilibrium constant for formation of the noncovalent complex between CheY and the phosphodonor, *k*<sub>phos</sub> is the rate constant for phosphotransfer within the noncovalent complex, and *k*<sub>dephos</sub> is the rate constant for CheY autodephosphorylation. Values for *k*<sub>phos</sub>/*K*<sub>S</sub>, the apparent bimolecular rate constant for autophosphorylation, were determined from the slopes of the linear plots.

**Ionic Strength Experiments.** For several of the CheY variants, *k*<sub>phos</sub>/*K*<sub>S</sub> values were determined at four different ionic strengths ranging from 0.23 to 1.63 M. Time courses were measured by stopped-flow fluorescence as described above. Both CheY and phosphodonor reaction solutions contained 100 mM Hepes (pH 7.0) and 10 mM MgCl<sub>2</sub>, and KCl was added to the protein and phosphodonor solutions to achieve the desired ionic strength. For each CheY variant and ionic strength condition, time courses were recorded at four different phosphodonor concentrations. Plots of *k*<sub>obs</sub> versus phosphodonor concentration were linear, and the slope gave *k*<sub>phos</sub>/*K*<sub>S</sub> values, exactly as described above for rate constants measured at ambient ionic strength. Each experimental condition (CheY variant and ionic strength) was examined in duplicate.

Quantitative analysis of the effects of ionic strength on CheY autophosphorylation kinetics was based on a published method.<sup>30</sup> For enzymatic reactions in which the formation of Coulombic interactions (long-range electrostatic interactions) is a kinetic determinant [e.g., formation of ion pairs between enzyme (E) and substrate (S)], increasing solution ionic strength slows the reaction due to charge screening effects of solution counterions. On the basis of polyelectrolyte theory and empirical support from the behavior of multiple enzymes,<sup>30–32</sup> plots of log<sub>10</sub>(*k*<sub>cat</sub>/*K*<sub>m</sub>) (or individual kinetic parameters) versus the log<sub>10</sub> of the concentration of monovalent salt are linear over a large ionic strength range. The slope of the resultant line is  $-n'$ , where *n'* approximates the number of counterions released from charged residues or substrate ions upon complex formation, which is usually reflective of the number of charges involved in salt bridges between the enzyme and substrate in the E-S complex (see the Supporting Information for additional details). For our studies, *k*<sub>phos</sub>/*K*<sub>S</sub> values for CheY autophosphorylation measured at different ionic strengths were first corrected for small differences in Mg<sup>2+</sup> binding affinities at different ionic strengths (see the Supporting Information). Then, for each CheY and phosphodonor pair, the log<sub>10</sub> values of the corrected *k*<sub>phos</sub>/*K*<sub>S</sub> values were plotted versus the log<sub>10</sub> of the total ionic strength of the reaction solution. The data were fit using linear regression (Prism) and slopes ( $-n'$  values) determined.

**Docking MPI into the CheY Variant Active Site.** Atomic coordinates for MPI were generated using the prodr server (<http://davapc1.bioch.dundee.ac.uk/prodr/>). Water and glycerol molecules and sulfate ions were removed from PDB entry 3FFW,<sup>25</sup> the PDB entry for the X-ray crystal structure of the CheY F14Q/N59Q/E89Y triple mutant complexed with BeF<sub>3</sub><sup>-</sup> and Mn<sup>2+</sup>. Using the Docking Wizard utility within the PyMOL Molecular Graphics System, version 1.1. (Schrödinger, LLC), the three phosphoryl oxygen atoms in MPI were superimposed on the three fluorine atoms in the BeF<sub>3</sub><sup>-</sup> anion bound to chain B of edited PDB entry 3FFW, with the imidazole oriented toward the solvent. With the phosphoryl oxygens being kept stationary, the torsional angle within MPI was rotated manually to minimize apparent steric overlap between the MPI and



**Table 1. Rate Constants for Autophosphorylation of Wild-Type and Mutant CheY with PAM or AcP<sup>a</sup>**

CheY designation	residue at position 14 (DD + 1)	residue at position 59 (D + 2)	residue at position 89 (T + 2)	$k_{\text{phos}}/K_S$ ( $\text{M}^{-1} \text{s}^{-1}$ ) <sup>b</sup>		PAM preference <sup>c</sup>
				PAM	AcP	
wild type	F	N	E	10 ± 0.50	11 ± 0.84	0.91
D + 2 Single Mutants						
RE	F	R	E	54 ± 1.6 <sup>d</sup>	7.6 ± 0.0 <sup>d</sup>	7.1
KE	F	K	E	32 ± 1.3	5.8 ± 0.35	5.5
ME	F	M	E	26 ± 4.8	1.3 ± 0.61	20
LE	F	L	E	12 ± 0.68	0.97 ± 0.12	12
AE	F	A	E	9.0 ± 0.21 <sup>d</sup>	1.3 ± 0.21 <sup>d</sup>	6.9
DE	F	D	E	3.7 ± 0.55	<0.2 <sup>e</sup>	>19
EE	F	E	E	2.7 ± 0.20	<0.2 <sup>e</sup>	>13
T + 2 Single Mutants						
NY	F	N	Y	240 ± 34	13 ± 1.9	18
NL	F	N	L	140 ± 21	33 ± 2.8	4.2
NR	F	N	R	93 ± 18	62 ± 5.5	1.5
NK	F	N	K	60 ± 7.3	42 ± 0.90	1.4
NH	F	N	H	30 ± 6.8	12 ± 2.1	2.5
NQ	F	N	Q	19 ± 0.28 <sup>d</sup>	36 ± 1.8 <sup>d</sup>	0.53
NA	F	N	A	10 ± 0.85 <sup>d</sup>	18 ± 2.0 <sup>d</sup>	0.55
D + 2/T + 2 Double Mutants						
KY	F	K	Y	370 ± 1.4	23 ± 1.5	16
MR	F	M	R	66 ± 1.3	18 ± 0.49	3.7
MK	F	M	K	97 ± 4.5	16 ± 1.1	6.1
EH	F	E	H	37 ± 2.1	2.3 ± 0.00	16
DL	F	D	L	71 ± 4.9	0.27 ± 0.058	260
DD + 1/D + 2/T + 2 Triple Mutants						
*KY	Q	K	Y	330 ± 4.7	25 ± 0.35	13
*MR	E	M	R	46 ± 0.71	9.5 ± 1.3	4.8

<sup>a</sup>Reaction conditions: 25 °C, pH 7.0, ionic strength of 230 mM, and 10 mM MgCl<sub>2</sub>. <sup>b</sup>Rate constants represent the average and standard deviation of at least two independent experiments. <sup>c</sup>Ratio of  $k_{\text{phos}}/K_S$  values for PAM and AcP. <sup>d</sup>Rates agree with previous measurements made at a single phosphodonor concentration.<sup>35,56</sup> <sup>e</sup>A  $k_{\text{phos}}/K_S$  value of 0.2  $\text{M}^{-1} \text{s}^{-1}$  is the estimated lower limit of detection for the assay.

CheY active site atoms and to allow solvent accessibility of the carbon atom corresponding to C $\gamma$  in phosphohistidine, as would be expected for the sensor kinase phosphohistidine phosphodonor. Hydrogen atoms were added to the resultant complex using Reduce,<sup>33</sup> and a dot image representing positive and negative interatomic interactions in the docked structure was generated using Probe.<sup>34</sup>

**Structure-Based Estimation of Nonpolar Surface Areas.** The nonpolar surface areas of residues at positions D + 2 (CheY residue 59) and T + 2 (CheY residue 89) were estimated on the basis of X-ray crystal structures. Of the eight amino acids found at positions D + 2 or T + 2 in the 19 tested CheY mutants that did not contain a substitution at position DD + 1 (CheY residue 14), five amino acids at position D + 2 and seven amino acids at position T + 2 are present in structures of CheY variants in the Protein Data Bank (1FQW, 1MIH, 3F7N, 3FFT, 3FFW, 3FFX, 3FGZ, 3RVJ, 3RVL, 3RVN, and 3RVP)<sup>11,25,35</sup> (C. A. Starbird, R. M. Immormino, R. E. Silversmith, and R. B. Bourret, unpublished observations). The conformation of the four remaining amino acids (Ala, Leu, and Glu at position D + 2 and Ala at position T + 2) were conservatively modeled using the BeF<sub>3</sub><sup>−</sup>-bound structure of wild-type CheY (PDB entry 1FQW)<sup>11</sup> as a scaffold. For example, the Ala side chains were modeled by terminating the wild-type side chains at the  $\beta$ -carbon. The resulting structures or models were then stripped of solvent molecules, except the divalent metal, and protonated using Reduce, and the van der Waals (VDW) surface for the residues surrounding the site of

phosphorylation was calculated with Probe.<sup>33,34</sup> The dot density for the VDW surface calculated by Probe was left at the default value of 16 dots per square angstrom. To determine if dots on the VDW surface belonged to the active site pocket or were external, a computer program was written that casts rays from a point in the center of the pocket (the nitrogen linked to the phosphorus of MPI docked to the CheY active site) outward to the dots on the VDW surface. Dots for which the rays could be drawn without passing through the VDW surface were assumed to be part of the active site. The active site surface dots belonging to nonpolar side chain atoms (carbon or hydrogen) were counted and divided by 16 to give the nonpolar surface areas for residue D + 2 or T + 2 in square angstroms. In cases where there was more than one crystal structure with the same residue at position D + 2 or T + 2, we used the average of the calculated surface areas for the residue from each structure. The total nonpolar surface areas for residues D + 2 and T + 2 were then determined by adding the nonpolar surface area values for particular amino acids at positions D + 2 and T + 2.

## RESULTS

**Nonconserved Active Site Residues Strongly Influence CheY Autophosphorylation Kinetics.** To assess the influence of variable active site residues in modulating catalysis of response regulator autophosphorylation, we measured pre-steady state kinetics for the reaction of a large set of CheY variants with AcP and PAM, representatives of the two

chemical classes of small molecule phosphodonors (Figure 1B). In all, 21 single, double, and triple mutants of CheY were analyzed. The great majority (19 of 21) were single or double mutants with substitutions at position D + 2 (CheY N59, two residues from the phosphorylated D57) and/or T + 2 (CheY E89, two residues from the conserved active site T87) (Figure 1A). The two remaining CheY variants were triple mutants with an additional substitution at position DD + 1 (CheY F14, the residue after the conserved D12-D13 pair). Specific substitutions were chosen to give a variety of chemical properties, and many also mimicked residues found at the corresponding positions in other well-studied receiver domains. For all of the reactions, stopped-flow fluorescence time courses that monitor the accumulation of phosphorylated CheY gave excellent fits to a single-exponential decay ( $R^2 > 0.99$ , with the great majority  $>0.999$ ), from which first-order rate constants ( $k_{\text{obs}}$ ) were obtained. Plots of  $k_{\text{obs}}$  versus phosphodonor concentration were linear for all combinations of CheY and phosphodonor, as has been previously observed for reactions of wild-type CheY with AcP and PAM.<sup>15,17</sup> Thus, there was no detectable binding between the phosphodonor and CheY ( $K_S \gg [\text{phosphodonor}]$ ) under the conditions used here. The slopes of the resultant lines gave the effective bimolecular rate constants ( $k_{\text{phos}}/K_S$ ) and are listed in Table 1.

This set of CheY mutants and phosphodonors gave  $k_{\text{phos}}/K_S$  values that spanned a  $>1800$ -fold range in magnitude (Table 1), demonstrating that the residues at positions D + 2 and T + 2 in receiver domain active sites can have a profound impact on autophosphorylation kinetics. Under these reaction conditions (pH 7.0 and ionic strength of 230 mM), wild-type CheY gave similar rates for reaction with AcP ( $11 \text{ M}^{-1} \text{ s}^{-1}$ ) and PAM ( $10 \text{ M}^{-1} \text{ s}^{-1}$ ). In contrast, all other CheY variants exhibited different rates for reaction with PAM and AcP, indicating that the substitutions affected aspects of the autophosphorylation reaction that are different for the two classes of phosphodonors.

#### Autophosphorylation of CheY D + 2 Single Mutants.

Replacement of the wild-type Asn at CheY position D + 2 with amino acids that varied in size and polarity gave autophosphorylation rates that spanned a  $>270$ -fold range. For reaction with PAM, the substitutions resulted in both rate increases (up to 5-fold) and decreases (up to 4-fold) relative to that of wild-type CheY. In contrast, the same substitutions all gave reduced rates for AcP. Strikingly, with the exception of wild-type CheY, CheY variants with Glu at position T + 2 and different amino acids at position D + 2 displayed the same rank order (D + 2 residues: R and K  $>$  M, L, and A  $>$  D and E) for reaction with both phosphodonors. This ranking suggests a correlation between increased positive charge at position D + 2 and faster autophosphorylation rates. Although an acidic side chain at position D + 2 was detrimental to reaction with both phosphodonors, the effect was especially severe for AcP, where CheY DE and CheY EE gave no detectable accumulation of CheY-P (Table 1). When the previously measured autodephosphorylation rates of CheY DE and CheY EE were taken into account,<sup>26</sup> both variants were determined to possess  $k_{\text{phos}}/K_S$  values for reaction with AcP below the measurable lower limit (Table 1). Thus, negative charge at both CheY positions D + 2 and T + 2 is extremely detrimental, if not prohibitive, for CheY autophosphorylation with AcP.

#### Autophosphorylation of CheY T + 2 Single Mutants.

The single-amino acid replacements of glutamate at CheY position T + 2 overwhelmingly gave enhanced rates of autophosphorylation with both phosphodonors, but especially

for PAM. Notably, CheY NY exhibited a 24-fold rate enhancement with PAM, whereas the same substitution gave a rate indistinguishable from that of wild-type CheY for reaction with AcP. The rank order for CheY proteins varying at position T + 2 for reaction with AcP (T + 2 residues: R and K  $>$  Q, L, and A  $>$  H, Y, and E) was similar to that observed for D + 2 variants, suggesting that positive charge at T + 2 also enhances the autophosphorylation rate. However, the rank order for the reaction of this set of CheY proteins with PAM was different (T + 2 residues: Y and L  $>$  R and K  $>$  H and Q  $>$  A and E), suggesting that large hydrophobic residues at position T + 2 may be advantageous for reaction with PAM, thus implicating other kinetic determinants besides side chain charge.

**Autophosphorylation of CheY DD + 1/D + 2/T + 2 Triple Mutants.** The two CheY triple mutants included in this study, CheY \*KY and CheY \*MR (Table 1), contained a substitution at position DD + 1 (CheY Phe14) in addition to positions D + 2 and T + 2 and were designed to mimic the active sites of *B. subtilis* Spo0F and *E. coli* PhoB, respectively. Both CheY triple mutants gave rates that were similar to that of the corresponding D + 2/T + 2 double mutants. Although they comprise a very small data set, these results suggest that, as is the case with autodephosphorylation,<sup>25,26</sup> residue DD + 1 does not appear to modulate autophosphorylation rates.

**Variation in Phosphodonor Preference.** Wild-type CheY displays nearly identical  $k_{\text{phos}}/K_S$  values for reactions with AcP and PAM at a standard ionic strength of 230 mM (Table 1) and thus has essentially no preference for one phosphodonor compared to another (PAM preference of  $\sim 1$ ). In contrast, there was a  $>500$ -fold variation in preference for PAM over AcP for the mutant set studied here, with preferences ranging from 0.5 to 260 (Table 1). A plot of  $\log(k_{\text{phos}}/K_S \text{ PAM})$  versus  $\log(k_{\text{phos}}/K_S \text{ AcP})$  (Figure 2) graphically illustrates the preference of all but two of the CheY mutants for PAM, as well as the diversity of magnitudes of the preference for PAM. For the two CheY variants (CheY NA and CheY NQ) that preferred AcP, the preference was weak (only 2-fold).

**MPI Further Enhances the Kinetics for Some CheY Variants.** PAM and AcP differ in both chemical linkage (and implicit charge) and size (Figure 1B). To probe the mechanistic basis for the general preference for PAM over AcP observed here, we measured the kinetics of autophosphorylation with MPI (monophosphoimidazole) for several CheY mutants that strongly preferred PAM over AcP. MPI has the same N–P chemical linkage (and thus similar charge distribution) as PAM but is larger than AcP. If size were the dominant deterring factor for AcP, then the order of the reaction rates would be as follows: PAM  $>$  AcP  $>$  MPI. However, rates for reaction with MPI were all at least as fast as those with PAM (Table 2), with several mutants exhibiting extremely large rate enhancements. Thus, the preference for PAM over AcP is not due to phosphodonor size but must be due to chemical linkage or charge.

Several of the CheY variants demonstrated strong preferences for MPI over PAM. In particular, CheY \*KY and CheY NY, both of which exhibited rates with PAM  $>20$ -fold faster than that of wild-type CheY, reacted with MPI another 16–130-fold faster than with PAM. The  $k_{\text{phos}}/K_S$  value for reaction of CheY \*KY with MPI ( $43000 \text{ M}^{-1} \text{ s}^{-1}$ ) represents the fastest autophosphorylation rate of this mutant set and is 4300-fold faster than the rate of wild-type CheY with AcP or PAM. In

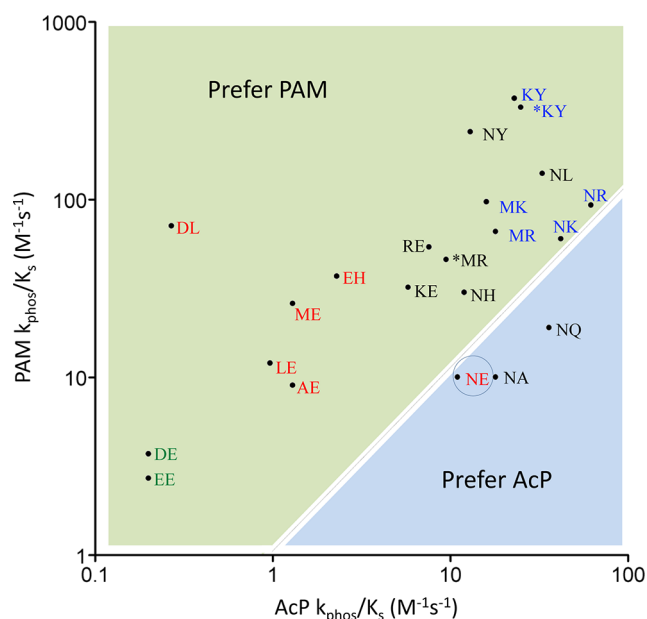


**Figure 2.** Phosphodonor preference (PAM vs AcP) for the set of CheY variants studied. For each CheY variant, the position of the point reflects the logarithms of the  $k_{\text{phos}}/K_s$  values (Table 1) for reaction with AcP (abscissa) or PAM (ordinate). CheY variants are designated by the amino acids at positions D + 2 and T + 2, with wild-type CheY (NE) circled. \*KY and \*MR have additional substitutions at position DD + 1 (F14Q and F14E) to mimic the Spo0F and PhoB response regulators, respectively. Designations are color-coded to reflect the net charge of residues at positions DD + 1, D + 2, and T + 2: blue for +1, black for 0, red for -1, and green for -2. The black dotted line (slope of 1) separates the plot into regions that prefer PAM (light green) or prefer AcP (light blue).

**Table 2. Rate Constants for Autophosphorylation of Selected CheY Variants with MPI, PAM, or AcP<sup>a</sup>**

residue at position D + 2	residue at position T + 2	$k_{\text{phos}}/K_s$ ( $\text{M}^{-1} \text{s}^{-1}$ )		
		MPI <sup>b</sup>	PAM <sup>c</sup>	AcP <sup>c</sup>
K	Y <sup>d</sup>	43000 ± 120	330	25
N	Y	3900 ± 470	240	13
E	H	440 ± 2.8	37	2.3
M	E	51 ± 7.0	26	1.3
D	E	2.5 ± 1.5	3.7	<0.2
N	E <sup>e</sup>	43 ± 2.8	10	11

<sup>a</sup>Reaction conditions: 25 °C, pH 7.0, ionic strength of 230 mM, and 10 mM MgCl<sub>2</sub>. <sup>b</sup>Values are the average and standard deviation of two independent measurements. <sup>c</sup>Values are from Table 1; see Table 1 for standard deviations. <sup>d</sup>The variant is CheY \*KY, the triple mutant with a glutamine at position DD + 1 (see Table 1). <sup>e</sup>Wild-type CheY.

addition to CheY \*KY and CheY NY, CheY EH also exhibited a further rate enhancement of >10-fold with MPI relative to its rate with PAM. Thus, instead of being a deterrent, the added bulk of MPI appeared to substantially increase autophosphorylation rates for three CheY variants relative to their rates with PAM. In contrast, CheY DE and CheY ME exhibited rates for MPI that were similar to their rates with PAM, indicating that MPI did not offer anything deleterious or advantageous over PAM for two CheY mutants. Thus, the large rate enhancements for MPI over PAM appeared to correlate with the presence of an aromatic group at the position T + 2.

**Docking MPI into the CheY \*KY Structure Reveals the Role of Steric Complementarity.** To explore the structural basis of the large rate enhancements for several CheY variants, especially CheY \*KY and CheY NY, with MPI, we docked the MPI molecule into the active site of CheY \*KY as described in Experimental Procedures. The X-ray crystal structure of CheY \*KY (PDB entry 3FFW)<sup>25</sup> complexed with Mn<sup>2+</sup> and the phosphoryl group analogue BeF<sub>3</sub><sup>-</sup> was used as a model of the active conformation, the probable reactive species in autophosphorylation.<sup>17,20,23</sup> The docked orientation (Figure 3) positioned the imidazole ring of the MPI and the aromatic

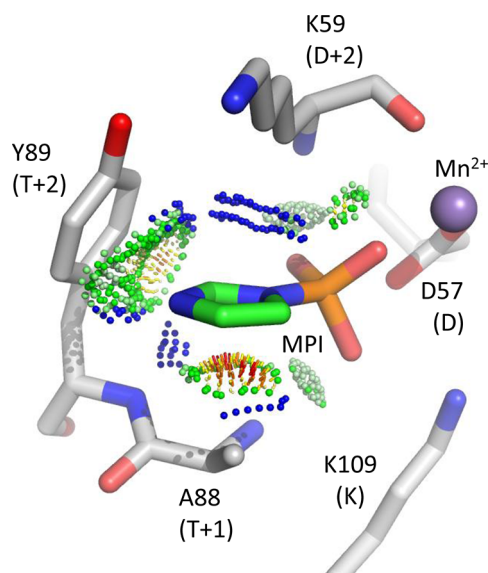


**Figure 3.** Model of MPI docked into the active site of the CheY \*KY·Mn<sup>2+</sup>·BeF<sub>3</sub><sup>-</sup> complex (PDB entry 3FFW).<sup>25</sup> Green and blue probe dots represent favorable van der Waals interactions, whereas orange and red dots represent steric clashes. The BeF<sub>3</sub><sup>-</sup> ion present in the original structure is not shown for the sake of clarity.

ring of the tyrosine at position T + 2 virtually perpendicular to one another in an optimal position for edge-to-face  $\pi$ - $\pi$  interactions.<sup>36</sup> In addition, there were a large number of van der Waals interactions between the imidazole group of MPI and both the tyrosine side chain at position T + 2 and the lysine at position D + 2. It is likely that similar interactions also occur in the other two CheY variants (CheY NY and CheY EH, both of which have an aromatic group at position T + 2) that show very fast reaction with MPI. Thus, the modeling suggested that enhanced binding between the phosphodonor and CheY due to an enlarged sterically complementary hydrophobic binding surface and  $\pi$ - $\pi$  interactions is a likely explanation for the greatly enhanced rates. The 10-fold increase in rate of CheY \*KY versus that of CheY NY may be due to a larger binding interface (K vs N) as well an additional positive charge (see below).

#### Statistical Correlations between D + 2/T + 2 Side Chain Properties and CheY Autophosphorylation Rates.

The trends discussed above suggested that increased positive charge of D + 2/T + 2 side chains or the presence of an aromatic side chain could be kinetic determinants that enhanced CheY autophosphorylation. To test these trends more rigorously and to gain insight into which factors may dominate for each of the two classes of phosphodonors, we conducted statistical analysis of rates for wild-type CheY and all

19 CheY single or double mutants for reaction with AcP or PAM. Plots relating net electrostatic charge or nonpolar surface area of residues D + 2 and T + 2 versus  $\log(k_{\text{phos}}/K_s)$  were generated for reaction with AcP or PAM (Figure 4). There was

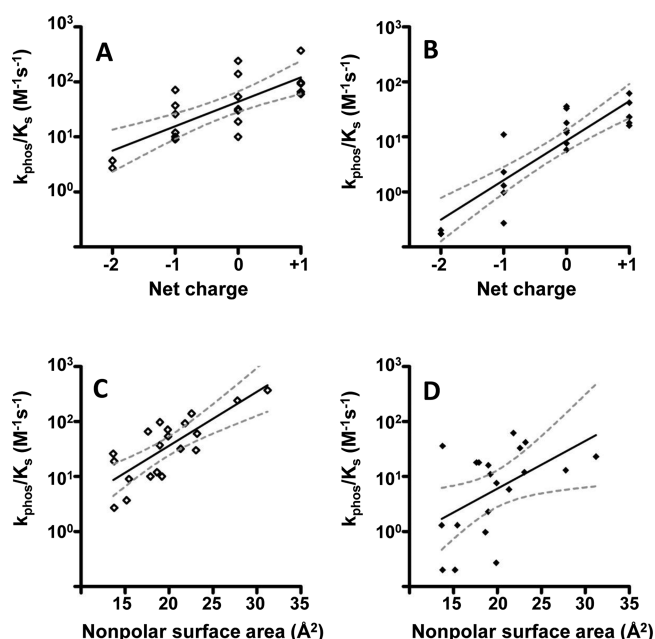


**Figure 4.** Correlations between net charge (A and B) or nonpolar surface area (C and D) at positions D + 2 and T + 2 and the measured rate constants [ $k_{\text{phos}}/K_s$  (from Table 1)] for autophosphorylation reactions with PAM (A and C) or AcP (B and D). Each point represents a single CheY variant. Net charge was calculated assuming histidyl residues are neutral. The nonpolar surface area was calculated as described in Experimental Procedures. For each plot, the black dashed line is the linear regression best-fit line and the gray dashed lines represent the 95% confidence bands.  $R^2$  values were 0.57, 0.76, 0.61, and 0.25 for panels A–D, respectively.

a significant Pearson correlation between net charge and  $\log(k_{\text{phos}}/K_s)$  for both PAM and AcP ( $p = 0.0001$  and  $p < 0.0001$ , respectively), supporting the notion that an increased positive charge enhances the rate for both AcP and PAM. Furthermore, the magnitudes of the slopes of the linear regression lines [0.44 for PAM and 0.72 for AcP (Figure 4A,B)] suggest that the charge effect was greater for AcP (−2 charge) than PAM (−1 charge), consistent with the observation that CheY EE and CheY DE gave no detectable reaction with AcP but reacted with PAM just modestly slower than with wild-type CheY. The two classes of phosphodonors also exhibited differences in correlations between  $\log(k_{\text{phos}}/K_s)$  and the nonpolar surface area of the active site “pocket” formed by the side chains of positions T + 2 and D + 2. For PAM, there was a strong Pearson correlation ( $p < 0.0001$ ) and the linear regression analysis showed a tight 95% confidence band, whereas for acetyl phosphate, the Pearson correlation was weak (but still significant;  $p = 0.0251$ ) and the linear regression exhibited a wide 95% confidence band (Figure 4C,D). Thus, CheY has different kinetic determinants for reaction with PAM or AcP. Overall, CheY autophosphorylation with PAM is more positively impacted by increasing the nonpolar surface area and less positively impacted by an increased charge than reaction with AcP.

**Effects of Ionic Strength on CheY Autophosphorylation Kinetics.** The correlation between the increased net charge of active site residues and faster autophosphorylation observed here (Figure 4A,B) implies a role for electrostatic forces in driving CheY autophosphorylation kinetics. Previous studies demonstrated that CheY autophosphorylation rates decrease with an increasing ionic strength.<sup>16</sup> Rates that are sensitive to ionic strength in this manner generally reflect bimolecular reaction steps in which two separated oppositely charged species come together to form an ionic interaction (long-range electrostatic interactions),<sup>30</sup> such as the association of a charged enzyme active site with an oppositely charged substrate.<sup>30,37</sup> Solution counterions act to shield the charged groups and prevent the interaction. To assess whether the rate differences observed for CheY D + 2/T + 2 substitutions (Table 1) were due to the same electrostatic interactions that lead to the ionic strength dependence, we measured the ionic strength dependencies of autophosphorylation rates for a subset of CheY variants and quantitatively analyzed the results.

Plots of  $\log(\text{ionic strength})$  versus  $\log(k_{\text{phos}}/K_s)$  for autophosphorylation of CheY NE, CheY RE, CheY NR, and CheY NY with either PAM or AcP approximated linearity (Figure 5), as predicted by polyelectrolyte theory.<sup>30</sup> In this

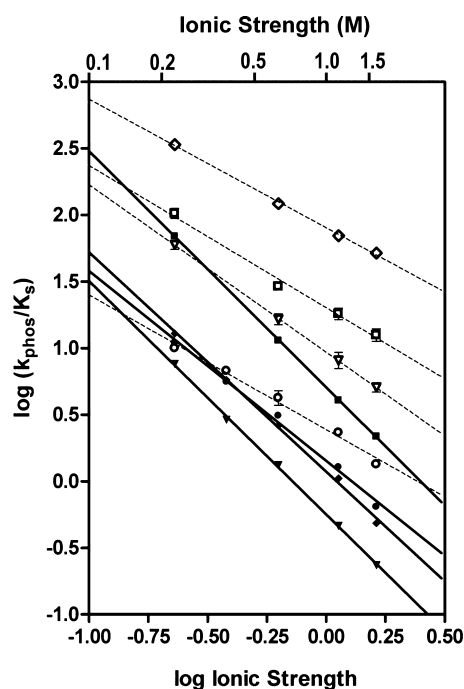


**Figure 5.** Ionic strength dependence of autophosphorylation rates for a subset of CheY variants. Filled symbols are for the reaction with AcP and empty symbols for the reaction with PAM. CheY variants are CheY NE (circles), CheY NY (diamonds), CheY RE (triangles), and CheY NR (squares), where the two letters designate the amino acids at positions D + 2 and T + 2 (CheY positions 59 and 89, respectively). Error bars represent the standard deviation from duplicate experiments.

analysis, for enzymes for which the rate of dissociation of the E·S complex is much faster than the chemical reaction step as occurs with CheY (see the Supporting Information), the absolute value of the slope of the linear relationship [ $n'$  (Table 3)] reflects the number of counterions displaced in the reaction step that is ionic strength sensitive. A priori, we might expect that, if the amino acid substitutions and ionic strength affected



**Table 3.  $n'$  Values Derived from Plots of Log(Ionic Strength) vs Log( $k_{\text{phos}}/K_s$ )**

residue at position D + 2	residue at position T + 2	$n'^a$	
		AcP	PAM
N	E <sup>b</sup>	1.4 ± 0.04	1.0 ± 0.05
R	E	1.8 ± 0.02	1.3 ± 0.06
N	R	1.8 ± 0.01	1.1 ± 0.06
N	Y	1.6 ± 0.03	0.97 ± 0.04

<sup>a</sup> $n'$  is the absolute value of the slope from Figure 5 and represents the number of counterions displaced on the protein or substrate in the reaction step(s) represented by  $k_{\text{phos}}/K_s$ . <sup>b</sup>Wild-type CheY.

the same long-range electrostatic interaction(s), then the kinetic differences between the mutants would diminish as ionic strength increased and the rates would eventually converge when all long-range electrostatic interactions were shielded by counterions. This would be reflected in different values of  $n'$  such that the variants with the fastest rates (at low ionic strengths) would have the largest ionic strength dependencies (highest  $n'$ ). However, the slopes for the various CheY variants were only modestly sensitive to the amino acid substitution but, instead, largely dependent on the phosphodonor (Table 3).  $n'$  values for all four CheY variants for reaction with PAM were close to unity (ranging from 0.97 to 1.3), which matches the net charge of  $-1$  of the PAM zwitterion (Figure 1B). In contrast, the  $n'$  values for reaction with AcP [net charge of  $-2$  (Figure 1B)] ranged from 1.4 to 1.8, and for each CheY variant,  $n'$  for AcP was between 1.4- and 1.7-fold greater than for PAM. The value of  $n'$  reflects the extent of the Coulombic interactions in the E·S complex and approximates the number of counterions released from charged residues and substrate ions upon complex formation, which is reflective of the number of charges involved in salt bridges between the enzyme and substrate in the E·S complex. The same qualitative result, that the CheY amino acid substitutions had small effects on the ionic strength sensitivity and that reactions with AcP had a 1.4–1.7-fold higher ionic strength sensitivity than those with PAM, was achieved with an alternative method of plotting the data whereby  $\log(k_{\text{phos}}/K_s)$  was plotted versus a term that included the square root of the ionic strength.<sup>38</sup>

The relative insensitivity of the  $n'$  values to amino acid substitution indicates that ionic strength and substitutions at positions D + 2 and T + 2 affect two different electrostatic phenomena. The correlation of the  $n'$  values with the  $-1$  and  $-2$  charges of the phosphodonors supports the notion that the ionic strength dependence reflects the binding of counterions to the phosphodonor anion to disrupt formation of an ion pair between the phosphodonor and a species that is common to all the mutant reactions, such as the CheY active site (see Discussion). Furthermore, because the amino acid substitutions had only small effects on the ionic strength sensitivities, the electrostatic component of the kinetic effects exerted by the substituted side chains likely does not involve long-range electrostatic interactions (i.e., separate charges coming together to form an ion pair). Instead, the side chains likely exert their effects via more localized electrostatic interactions that would not be susceptible to the effects of bulk solvent.

## DISCUSSION

Although response regulator autophosphorylation was discovered more than 20 years ago<sup>4</sup> and has since been established as having physiological relevance for multiple response regulators,<sup>5,6</sup> the reaction kinetics have been rigorously characterized only for CheY.<sup>15–18</sup> Prior to this study, the ranges of reaction rates and phosphodonor discrimination possible with the response regulator scaffold were unknown. As summarized in this section, there are now specific proposed mechanisms for the modulation of the catalysis of CheY phosphorylation that can be tested for generality in other response regulators, as well as in sensor kinase–response regulator pairs.

Specifically, this study provided substantial insight into the precise mechanisms by which electrostatic and steric interactions influence the kinetics of CheY autophosphorylation. We demonstrated that two types of electrostatic interactions affect reaction kinetics: long-range (getting the phosphodonor into the active site) and short-range (interactions between the active site and the phosphodonor once the enzyme–substrate complex has formed). Furthermore, the “direction” of long- and short-range electrostatic interactions is the same; both are enhanced by positive charge in the CheY active site. With regard to steric effects, the generally faster reaction rates observed with PAM compared to those of AcP were not attributable to the smaller size of PAM. Instead, the data provided strong evidence that aromatic/bulky hydrophobic groups in the CheY active site can interact directly with the imidazole portion of MPI (or the nitrogen atom of PAM) to increase binding energy and thus enhance phosphorylation rate.

**Phosphoramidates and Acyl Phosphates Have Different Kinetic Determinants.** Amino acid substitutions at positions D + 2 and T + 2 modulated CheY autophosphorylation rates by 2–3 orders of magnitude for each of the three phosphodonors tested (Tables 1 and 2). Multiple lines of evidence support the notion that CheY and other receiver domains exist as an equilibrium between multiple conformational states<sup>39,40</sup> and that the activated conformations autophosphorylate at an enhanced rate.<sup>17,23</sup> Thus, a change in rate as a result of substitution might reflect the effect of the substitution on the equilibrium between active and inactive conformational states.<sup>17,20</sup> However, simply changing the fraction of CheY in the activated conformation would manifest in rates changing in concert for all phosphodonors. In contrast, a central observation here was that the effect of substitutions at positions D + 2 and T + 2 on CheY autophosphorylation kinetics was phosphodonor-dependent (Tables 1 and 2 and Figure 2). With the inclusion of MPI, kinetic preferences for different phosphodonors for a single CheY variant were as high as 1700. Thus, the conformational state does not appear to be a dominant source of rate modulation for this mutant set. Furthermore, we probed the effect of conformational change on two of the CheY variants with enhanced rates of autophosphorylation. Both variants (CheY NR and NL) exhibited additional rate enhancements, similar in magnitude to that shown by wild-type CheY, when pushed into the activated conformation by binding to the FliM<sub>1–16</sub> peptide (Table S2 of the Supporting Information).

If conformation is not playing a dominant role in autophosphorylation rate modulation, then what is? Correlations between measured rate constants and chemical properties of the D + 2/T + 2 substitutions allowed us to propose several



kinetic determinants to account for the observed rate differences. Specifically, the increased positive charge and increased nonpolar surface area of the D + 2/T + 2 side chains both correlated with enhanced autophosphorylation rates (Figure 4). The analysis further revealed that the different phosphodonor classes were affected differentially by the kinetic determinants. Increased positive charge enhanced the autophosphorylation rate for both AcP and PAM but did so to a greater degree for AcP. Moreover, because the reaction with AcP displayed a stronger dependence on ionic strength than that with PAM (Figure 5), the preference for PAM over AcP for any mutant would be dependent on ionic strength. Increased nonpolar surface area strongly correlated with a faster rate of reaction with PAM, but the correlation for reaction with AcP was weak. Reaction with MPI showed yet a larger impact of nonpolar surface area than that of PAM. A plot of  $\log(k_{\text{phos}}/K_S)$  versus nonpolar surface area for the small set of mutants for which we measured reaction rates with MPI gave a linear regression line with a slope >2-fold higher than with PAM (data not shown). The differential impacts of kinetic determinants upon reaction with different phosphodonors underlie the variation in phosphodonor preference.

**Electrostatic Interactions Modulate CheY Autophosphorylation at Multiple Levels.** The correlation between the charge of the D + 2/T + 2 side chains and reaction rate identified a role for electrostatic interactions in the differing autophosphorylation kinetics of the CheY variants. However, the similar ionic strength sensitivities of the CheY variants suggested at least two electrostatic phenomena: one that was ionic strength sensitive and one that was ionic strength insensitive but sensitive to the charge at positions D + 2 and T + 2. Furthermore, quantitative analysis (Figure 5 and Table 3) revealed that the magnitude of the ionic strength sensitivity ( $n'$ ) was greater for AcP (net charge of  $-2$ ) than for PAM (net charge of  $-1$ ).  $n'$  values reflect the number of counterions released from charged species to form a noncovalent complex.

**Ionic Strength Inhibits Long-Range Electrostatic Interactions between a Positively Charged Active Site and a Negatively Charged Substrate.** Taken together, the observations summarized in the preceding paragraph provide compelling evidence that the ionic strength sensitive step involves direct interaction of the phosphodonor anion with a positively charged species that is common to the reactions for all the CheY variants. Calculation of the electrostatic surface potential of the CheY·Mg<sup>2+</sup> active site reveals a positively charged surface centered on the Mg<sup>2+</sup> and conserved lysine residue, which more than neutralizes the three conserved aspartyl residues (Adaptive Poisson–Boltzmann Solver;<sup>41</sup> PDB entry 2CHE<sup>42</sup> or 1FQW<sup>11</sup>). Structures of phosphatases within the haloacid dehalogenase superfamily (which have virtually identical active sites and catalyze the same chemistry as receiver domains) complexed with substrate analogues show two salt bridges between phosphoryl group oxygen atoms and Mg<sup>2+</sup> and the conserved Lys.<sup>12,43</sup> Therefore, a likely candidate for the ionic strength sensitive step in CheY autophosphorylation is the initial binding of the phosphodonor to CheY, which would involve formation of salt bridges between phosphoryl group oxygen anions and the Mg<sup>2+</sup> and lysyl cations. This suggests that the inhibitory effect of increasing ionic strength on  $k_{\text{phos}}/K_S$  would reflect an increase in  $K_S$  (weaker binding) rather than a decrease in  $k_{\text{phos}}$  and is consistent with the notion that ionic strength generally affects long-range electrostatic interactions. We also considered and rejected an alternate possibility that

noncovalent complexes formed between Mg<sup>2+</sup> and phosphodonor function as the reactive species in autophosphorylation and that ionic strength disrupts complex formation (see the Supporting Information).

The magnitudes of the  $n'$  values measured here deserve further comment. The agreement between  $n'$  values for reactions with PAM ( $\sim 1$ ) and the net charge of PAM ( $-1$ ) was striking as  $n'$  should approximate the number of counterions released from charged residues or substrate ions that interact. However, PAM is a zwitterion (Figure 1B), and the observation that PAM behaves more like a species with a charge of  $-1$  than a species with a charge of  $-2$  suggests that the positively charged nitrogen atom inhibits the ability of the K<sup>+</sup> counterions to bind to phosphoryl oxygens on PAM. Although  $n'$  values for reaction with AcP were 1.4–1.8-fold higher than for PAM, they did not reach the theoretical value of  $\sim 2$  expected for release of two counterions from AcP. This is similar to studies with RNase A in which  $n'$  increased linearly with substrate charge but with a slope of only  $\sim 0.2$  ( $n'/\text{charge}$ ). The  $n'/\text{charge}$  ratio of  $<1$  was attributed to uneven counterion density on the substrate,<sup>30</sup> which would be expected for AcP.

**Residues at Positions D + 2 and T + 2 Affect Localized Electrostatic Interactions.** The electrostatic interactions implicated by the correlation between the positive charge at positions D + 2 and T + 2 and enhanced rate were virtually insensitive to ionic strength. Thus, these interactions are likely to be more localized and not involve two separated and solvated charged species coming together to form an ion pair. The locations of the D + 2 and T + 2 side chains in the active site further indicate that these interactions likely involve energetics in the leaving group region of the autophosphorylation reaction. The D + 2 and T + 2 side chains are positioned near the leaving group atom bonded to the phosphorus, which is different for the phosphodonor classes. The leaving group for PAM is NH<sub>3</sub> (neutral), and the nitrogen atom carries a partial positive charge in the transition state. In contrast, the leaving group for AcP is acetate (charge of  $-1$ ), and the oxygen atom has a partial negative charge in the transition state. Thus, it is reasonable that the positive charge at position D + 2 or T + 2 may help stabilize the transition state of AcP more so than PAM via electrostatic attractive forces between positively charged side chain(s) and the leaving group atom. This is consistent with the observation that the slopes of the linear correlation between net positive charge and rate were higher and the correlations were statistically stronger for AcP than for PAM (Figure 4A,B). Similar roles of stabilizing negative charges in the transition state have been proposed for arginine residues that are prevalent in active sites of phosphotransfer enzymes.<sup>44</sup> Thus, electrostatic interactions caused by D + 2/T + 2 substitutions likely affect the  $k_{\text{phos}}$  component of  $k_{\text{phos}}/K_S$ .

**Nonpolar Surface Area and Steric Complementarity.** The overall preference of PAM over AcP for this CheY mutant set is consistent with accounts in the literature of receiver domains that react readily with PAM but do not react with AcP.<sup>4,21</sup> PAM and AcP have similar kinetics of hydrolysis in the absence of a catalyst,<sup>13,14</sup> so the preference for PAM is not due to an innately higher reactivity of PAM. In the mutant set studied here, reaction with PAM improved as the nonpolar surface became larger but AcP did not appear to benefit similarly. This was particularly evident in three CheY variants with tyrosine residues at position T + 2 (CheY NY, CheY KY, and CheY \*KY), which displayed greatly enhanced rates with

PAM that were not achievable with AcP. CheY NY and CheY \*KY underwent dramatic further rate enhancements with MPI (Table 2), and docking showed a strong likelihood of steric complementarity between MPI and both the D + 2 and T + 2 side chains (Figure 3). Why did AcP not similarly benefit from the added nonpolar surface area? Interestingly, docking of AcP into the active site of CheY \*KY (as shown in Figure 3 for MPI) showed that the planar -COCH<sub>3</sub> group linked to the phosphoryl group in AcP clashed with multiple atoms of the D + 2 and T + 2 side chain in all possible rotamers. In MPI, the planar imidazole is one atom closer to the phosphoryl group and so fits more snugly in the active site. These trends likely reflect a trade-off between enhanced surface for potential interaction with the limitation that the increased bulk does not introduce steric clash.

Finally, in addition to steric complementarity, the observed correlation between nonpolar surface area and autophosphorylation rate also likely reflects energetic contributions of providing a more hydrophobic environment for catalysis of the phosphotransfer reaction. A more hydrophobic active site pocket would result in strengthening the multiple types of electrostatic interactions that drive the reaction (described above) due to a decrease in the local dielectric constant.<sup>45</sup>

**Highly Accelerated Reactions between CheY Variants and MPI May Reflect the Structural Mimicry of Phosphotransfer from Sensor Kinases.** In two-component systems, the phosphohistidyl-containing domain that transfers directly to the receiver can be either a “dimerization and histidine phosphotransfer” (DHP) domain (present in canonical sensor kinases) or a “histidine-containing phosphotransfer” (HPT) domain (commonly found in phosphorelays and chemotaxis systems), both of which are four-helix bundles. Phosphotransfer from both DHP<sup>46,47</sup> and HPT<sup>19,48</sup> domains to response regulators occurs rapidly with rate constants of approximately  $\geq 10^6$  M<sup>-1</sup> s<sup>-1</sup>. Whereas previously determined autophosphorylation rates for wild-type CheY were  $\sim 10^5$  times slower than rates of transfer from cognate proteins, the rate constant for CheY \*KY autophosphorylation with MPI ( $4.3 \times 10^4$  M<sup>-1</sup> s<sup>-1</sup>) measured here approaches rates seen with the protein domains. Could interactions between the imidazole side chain and D + 2/T + 2 side chain atoms predicted by docking also occur in complexes between phosphorylated histidine kinases and response regulators? In the docked structure (Figure 3), the monophosphoimidazole carbon atom corresponding to histidyl C $\gamma$  is facing the solvent, allowing plenty of room for the rest of the histidyl side chain. Assessment of  $\sim 14000$  response regulator sequences showed that  $\sim 35\%$  have an aromatic residue (F, Y, W, or H) at position T + 2,<sup>22</sup> so these interactions could be common. Indeed, in the cocrystal structure of the HPT/response regulator pair YPD1/SLN1-R1 (PDB entry 2R25),<sup>49</sup> there is a phenylalanine at the SLN1-R1 T + 2 position that interacts with the conserved histidyl imidazole in YPD1, providing evidence that very similar interactions may help mediate binding between the HPT domain and the response regulator. In the HK853/RR468 complex between a kinase DHP domain and a cognate receiver, the imidazole group of the conserved His forms one end of a sandwich of van der Waals interactions with receiver domain residues D + 2 (Met) and T + 2 (Lys).<sup>50</sup> In the low-resolution complex between the DHP domain of the TrpA kinase and the TrpA response regulator (PDB entry 3AOR),<sup>51</sup> TrpA T + 2 Y82 interacts with ThkA H547 via parallel  $\pi$ - $\pi$  stacking interactions, but there is uncertainty in this exact alignment

because of weak electron density in this region. Thus, there may be multiple modes of interaction between D + 2/T + 2 side chains and the histidyl group, including direct interaction between an aromatic response regulator T + 2 side chain and the conserved histidyl side chain from the partner protein. It is likely that these interactions not only help to stabilize the kinase/receiver complex but also could strengthen the electrostatic interactions within the transition state by providing a more hydrophobic environment.

**Roles of Response Regulator Nonconserved Active Site Residues D + 2 and T + 2.** The influence of residues D + 2 and T + 2 on CheY autophosphorylation kinetics established here represents yet another example of the impact of these two positions on receiver domain phosphorylation reactions. Located at the “gateway” of the active site, residues D + 2 and T + 2 also play roles in sensor kinase recognition and binding,<sup>50,52,53</sup> receiver domain autodephosphorylation kinetics,<sup>25,26</sup> and phosphatase binding and catalysis.<sup>35,54,55</sup> Bioinformatics analysis of 1555 receiver domain sequences<sup>52</sup> reveals strong evolutionary covariation between residues at positions D + 2 and T + 2 (M. Laub, personal communication), consistent with a functional role for these positions in differentiating response regulator receiver domain functions.

Although amino acid substitutions at positions D + 2 and T + 2 had large effects on the kinetics and specificity of CheY autophosphorylation, other nonconserved active site positions likely also modulate response regulator autophosphorylation. For example, residue T + 1 is hypothesized to control access to the phosphorylation site.<sup>24</sup> Identification of all major determinants of response regulator phosphorylation chemistry and characterization of the interactions between such factors will require additional investigation.

## ■ ASSOCIATED CONTENT

### ● Supporting Information

Mg<sup>2+</sup> binding constants for select CheY variants (Table S1), rate constants in the presence of the FlIM peptide (Table S2), an addendum to Experimental Procedures (describing corrections made to autophosphorylation rates at different ionic strengths due to differences in Mg<sup>2+</sup> affinity and additional details describing the method of quantitation of ionic strength effects), and an addendum to the Discussion describing consideration of a possible role for soluble complexes between acetyl phosphate and Mg<sup>2+</sup> in autophosphorylation rate modulation. This material is available free of charge via the Internet at <http://pubs.acs.org>.

## ■ AUTHOR INFORMATION

### Corresponding Author

\*E-mail: [silversr@med.unc.edu](mailto:silversr@med.unc.edu). Telephone: (919) 966-2679. Fax: (919) 962-8103.

### Funding

Research reported in this publication was supported by the National Institute of General Medical Sciences of the National Institutes of Health via Grant R01GM050860.

### Notes

The authors declare no competing financial interest.

## ■ ACKNOWLEDGMENTS

We thank Dr. Ashalla Freeman, Dr. Yael Pazy-Benhar, Rachel Creager-Allen, and Stephani Page for helpful discussions and Dr. Mike Laub (Massachusetts Institute of Technology,

Cambridge, MA) for sharing covariation analysis results. We also thank Dr. Rick Stewart (University of Maryland, College Park, MD) and Dr. Gideon Schreiber (Weizmann Institute, Rehovot, Israel) for thoughtful discussion regarding analysis of the ionic strength effects.

## ABBREVIATIONS

AcP, acetyl phosphate; PAM, phosphoramidate; MPI, monophosphoimidazole; DD, two conserved acid residues on the receiver domain  $\beta 1\alpha 1$  loop that chelate the  $Mg^{2+}$  (D12 and D13 for *E. coli* CheY); D, conserved phosphorylated aspartate on  $\beta 3\alpha 3$  (D57 for CheY); T, conserved threonine/serine on  $\beta 4\alpha 4$  (T87 for CheY); K, conserved lysine on  $\beta 5\alpha 5$  (K109 for CheY); DD + 1, D + 2, and T + 2, nonconserved residues positioned one or two residues carboxyl terminal to DD, D, and T, respectively (F14, N59, and E89, respectively, for CheY); CheY XY, CheY double mutant where X and Y are the identities of the residues at positions D + 2 (residue 59 in CheY) and T + 2 (residue 89 in CheY), respectively; CheY \*XY, CheY triple mutant where X and Y are the identities of the residues at positions D + 2 (residue 59) and T + 2 (residue 89), respectively, with an additional substitution at position DD + 1.

## REFERENCES

- (1) Bourret, R. B., and Silversmith, R. E. (2010) Two-component signal transduction. *Curr. Opin. Microbiol.* 13, 113–115.
- (2) Capra, E. J., and Laub, M. T. (2012) Evolution of two-component signal transduction systems. *Annu. Rev. Microbiol.* 66, 325–347.
- (3) Galperin, M. Y. (2010) Diversity of structure and function of response regulator output domains. *Curr. Opin. Microbiol.* 13, 150–159.
- (4) Lukat, G. S., McCleary, W. R., Stock, A. M., and Stock, J. B. (1992) Phosphorylation of bacterial response regulator proteins by low molecular weight phospho-donors. *Proc. Natl. Acad. Sci. U.S.A.* 89, 718–722.
- (5) Wolfe, A. J. (2005) The acetate switch. *Microbiol. Mol. Biol. Rev.* 69, 12–50.
- (6) Wolfe, A. J. (2010) Physiologically relevant small phosphodonors link metabolism to signal transduction. *Curr. Opin. Microbiol.* 13, 204–209.
- (7) Bourret, R. B., Thomas, S. A., Page, S. C., Creager-Allen, R. L., Moore, A. M., and Silversmith, R. E. (2010) Measurement of response regulator autodephosphorylation rates spanning six orders of magnitude. *Methods Enzymol.* 471, 89–114.
- (8) Buckler, D. R., and Stock, A. M. (2000) Synthesis of [ $^{32}P$ ]phosphoramidate for use as a low molecular weight phosphodonor reagent. *Anal. Biochem.* 283, 222–227.
- (9) Gao, R., Tao, Y., and Stock, A. M. (2008) System-level mapping of *Escherichia coli* response regulator dimerization with FRET hybrids. *Mol. Microbiol.* 69, 1358–1372.
- (10) Bourret, R. B. (2010) Receiver domain structure and function in response regulator proteins. *Curr. Opin. Microbiol.* 13, 142–149.
- (11) Lee, S. Y., Cho, H. S., Pelton, J. G., Yan, D., Berry, E. A., and Wemmer, D. E. (2001) Crystal structure of activated CheY. Comparison with other activated receiver domains. *J. Biol. Chem.* 276, 16425–16431.
- (12) Wang, W., Cho, H. S., Kim, R., Jancarik, J., Yokota, H., Nguyen, H. H., Grigoriev, I. V., Wemmer, D. E., and Kim, S. H. (2002) Structural characterization of the reaction pathway in phosphoserine phosphatase: Crystallographic “snapshots” of intermediate states. *J. Mol. Biol.* 319, 421–431.
- (13) Chanley, J. D., and Feageson, E. (1963) A study of hydrolysis of phosphoramides. II. Solvolysis of phosphoramidic acid and comparison with phosphate esters. *J. Am. Chem. Soc.* 85, 1181–1190.

- (14) Koshland, D. E. (1952) Effect of catalysts on the hydrolysis of acetyl phosphate. Nucleophilic displacement mechanisms in enzymic reactions. *J. Am. Chem. Soc.* 74, 2286–2296.
- (15) Da Re, S. S., Deville-Bonne, D., Tolstykh, T., Veron, M., and Stock, J. B. (1999) Kinetics of CheY phosphorylation by small molecule phosphodonors. *FEBS Lett.* 457, 323–326.
- (16) Mayover, T. L., Halkides, C. J., and Stewart, R. C. (1999) Kinetic characterization of CheY phosphorylation reactions: Comparison of P-CheA and small-molecule phosphodonors. *Biochemistry* 38, 2259–2271.
- (17) Schuster, M., Silversmith, R. E., and Bourret, R. B. (2001) Conformational coupling in the chemotaxis response regulator CheY. *Proc. Natl. Acad. Sci. U.S.A.* 98, 6003–6008.
- (18) Silversmith, R. E., Appleby, J. L., and Bourret, R. B. (1997) Catalytic mechanism of phosphorylation and dephosphorylation of CheY: Kinetic characterization of imidazole phosphates as phosphodonors and the role of acid catalysis. *Biochemistry* 36, 14965–14974.
- (19) Stewart, R. C., Jahreis, K., and Parkinson, J. S. (2000) Rapid phosphotransfer to CheY from a CheA protein lacking the CheY-binding domain. *Biochemistry* 39, 13157–13165.
- (20) Barbieri, C. M., Mack, T. R., Robinson, V. L., Miller, M. T., and Stock, A. M. (2010) Regulation of response regulator autophosphorylation through interdomain contacts. *J. Biol. Chem.* 285, 32325–32335.
- (21) Zapf, J. W., Hoch, J. A., and Whiteley, J. M. (1996) A phosphotransferase activity of the *Bacillus subtilis* sporulation protein Spo0F that employs phosphoramidate substrates. *Biochemistry* 35, 2926–2933.
- (22) Ulrich, L. E., and Zhulin, I. B. (2010) The MiST2 database: A comprehensive genomics resource on microbial signal transduction. *Nucleic Acids Res.* 38, D401–D407.
- (23) Ames, S. K., Frankema, N., and Kenney, L. J. (1999) C-terminal DNA binding stimulates N-terminal phosphorylation of the outer membrane protein regulator OmpR from *Escherichia coli*. *Proc. Natl. Acad. Sci. U.S.A.* 96, 11792–11797.
- (24) Volz, K. (1993) Structural conservation in the CheY superfamily. *Biochemistry* 32, 11741–11753.
- (25) Pazy, Y., Wollish, A. C., Thomas, S. A., Miller, P. J., Collins, E. J., Bourret, R. B., and Silversmith, R. E. (2009) Matching biochemical reaction kinetics to the timescales of life: Structural determinants that influence the autodephosphorylation rate of response regulator proteins. *J. Mol. Biol.* 392, 1205–1220.
- (26) Thomas, S. A., Brewster, J. A., and Bourret, R. B. (2008) Two variable active site residues modulate response regulator phosphoryl group stability. *Mol. Microbiol.* 69, 453–465.
- (27) Boesch, K. C., Silversmith, R. E., and Bourret, R. B. (2000) Isolation and characterization of nonchemotactic CheZ mutants of *Escherichia coli*. *J. Bacteriol.* 182, 3544–3552.
- (28) Sheridan, R. C., McCullough, J. F., Wakefield, Z. T., Allcock, H. R., and Walsh, E. J. (1971) Phosphoramidic acid and its salts. *Inorg. Synth.* 13, 23–26.
- (29) Rathlev, T., and Rosenberg, T. (1956) Non-enzymic formation and rupture of phosphorus to nitrogen linkages in phosphoramido derivatives. *Arch. Biochem. Biophys.* 65, 319–339.
- (30) Park, C., and Raines, R. T. (2001) Quantitative analysis of the effect of salt concentration on enzymatic catalysis. *J. Am. Chem. Soc.* 123, 11472–11479.
- (31) Hicks, S. N., Smiley, R. D., Hamilton, J. B., and Howell, E. E. (2003) Role of ionic interactions in ligand binding and catalysis of R67 dihydrofolate reductase. *Biochemistry* 42, 10569–10578.
- (32) Plantinga, M. J., Korennykh, A. V., Piccirilli, J. A., and Correll, C. C. (2008) Electrostatic interactions guide the active site face of a structure-specific ribonuclease to its RNA substrate. *Biochemistry* 47, 8912–8908.
- (33) Word, J. M., Lovell, S. C., Richardson, J. S., and Richardson, D. C. (1999) Asparagine and glutamine: Using hydrogen atom contacts in the choice of side-chain amide orientation. *J. Mol. Biol.* 285, 1735–1747.



- (34) Chen, V. B., Arendall, W. B., III, Headd, J. J., Keedy, D. A., Immormino, R. M., Kapral, G. J., Murray, L. W., Richardson, J. S., and Richardson, D. C. (2010) MolProbity: All-atom structure validation for macromolecular crystallography. *Acta Crystallogr. D* 66, 12–21.
- (35) Silversmith, R. E., Guanga, G. P., Betts, L., Chu, C., Zhao, R., and Bourret, R. B. (2003) CheZ-mediated dephosphorylation of the *Escherichia coli* chemotaxis response regulator CheY: Role for CheY glutamate 89. *J. Bacteriol.* 185, 1495–1502.
- (36) Meyer, E. A., Castellano, R. K., and Diederich, F. (2003) Interactions with aromatic rings in chemical and biological recognition. *Angew. Chem., Int. Ed.* 42, 1210–1250.
- (37) Sines, J. J., Allison, S. A., and McCammon, J. A. (1990) Point charge distributions and electrostatic steering in enzyme/substrate encounter: Brownian dynamics of modified copper/zinc superoxide dismutases. *Biochemistry* 29, 9403–9412.
- (38) Schreiber, G., and Fersht, A. R. (1996) Rapid, electrostatically assisted association of proteins. *Nat. Struct. Biol.* 3, 427–431.
- (39) McDonald, L. R., Boyer, J. A., and Lee, A. L. (2012) Segmental motions, not a two-state concerted switch, underlie allostery in CheY. *Structure* 20, 1363–1373.
- (40) Stock, A. M., and Guhaniyogi, J. (2006) A new perspective on response regulator activation. *J. Bacteriol.* 188, 7328–7330.
- (41) Baker, N. A., Sept, D., Joseph, S., Holst, M. J., and McCammon, J. A. (2001) Electrostatics of nanosystems: Application to microtubules and the ribosome. *Proc. Natl. Acad. Sci. U.S.A.* 98, 10037–10041.
- (42) Stock, A. M., Martinez-Hackert, E., Rasmussen, B. F., West, A. H., Stock, J. B., Ringe, D., and Petsko, G. A. (1993) Structure of the  $Mg^{2+}$ -bound form of CheY and mechanism of phosphoryl transfer in bacterial chemotaxis. *Biochemistry* 32, 13375–13380.
- (43) Roberts, A., Lee, S. Y., McCullagh, E., Silversmith, R. E., and Wemmer, D. E. (2005) YbiV from *Escherichia coli* K12 is a HAD phosphatase. *Proteins* 58, 790–801.
- (44) Lassila, J. K., Zalatan, J. G., and Herschlag, D. (2011) Biological phosphoryl-transfer reactions: Understanding mechanism and catalysis. *Annu. Rev. Biochem.* 80, 669–702.
- (45) Janin, J., and Chothia, C. (1976) Stability and specificity of protein-protein interactions: The case of the trypsin-trypsin inhibitor complexes. *J. Mol. Biol.* 100, 197–211.
- (46) Groban, E. S., Clarke, E. J., Salis, H. M., Miller, S. M., and Voigt, C. A. (2009) Kinetic buffering of cross talk between bacterial two-component sensors. *J. Mol. Biol.* 390, 380–393.
- (47) Skerker, J. M., Prasol, M. S., Perchuk, B. S., Biondi, E. G., and Laub, M. T. (2005) Two-component signal transduction pathways regulating growth and cell cycle progression in a bacterium: A system-level analysis. *PLoS Biol.* 3, e334.
- (48) Janiak-Spens, F., Cook, P. F., and West, A. H. (2005) Kinetic analysis of YPD1-dependent phosphotransfer reactions in the yeast osmoregulatory phosphorelay system. *Biochemistry* 44, 377–386.
- (49) Zhao, X., Copeland, D. M., Soares, A. S., and West, A. H. (2008) Crystal structure of a complex between the phosphorelay protein YPD1 and the response regulator domain of SLN1 bound to a phosphoryl analog. *J. Mol. Biol.* 375, 1141–1151.
- (50) Casino, P., Rubio, V., and Marina, A. (2009) Structural insight into partner specificity and phosphoryl transfer in two-component signal transduction. *Cell* 139, 325–336.
- (51) Yamada, S., Akiyama, S., Sugimoto, H., Kumita, H., Ito, K., Fujisawa, T., Nakamura, H., and Shiro, Y. (2006) The signaling pathway in histidine kinase and the response regulator complex revealed by X-ray crystallography and solution scattering. *J. Mol. Biol.* 362, 123–139.
- (52) Skerker, J. M., Perchuk, B. S., Siryaporn, A., Lubin, E. A., Ashenberg, O., Goulian, M., and Laub, M. T. (2008) Rewiring the specificity of two-component signal transduction systems. *Cell* 133, 1043–1054.
- (53) Szurmant, H., and Hoch, J. A. (2010) Interaction fidelity in two-component signaling. *Curr. Opin. Microbiol.* 13, 190–197.
- (54) Pazy, Y., Motaleb, M. A., Guarnieri, M. T., Charon, N. W., Zhao, R., and Silversmith, R. E. (2010) Identical phosphatase mechanisms achieved through distinct modes of binding phosphoprotein substrate. *Proc. Natl. Acad. Sci. U.S.A.* 107, 1924–1929.
- (55) Zhao, R., Collins, E. J., Bourret, R. B., and Silversmith, R. E. (2002) Structure and catalytic mechanism of the *E. coli* chemotaxis phosphatase CheZ. *Nat. Struct. Biol.* 9, 570–575.
- (56) Silversmith, R. E., Smith, J. G., Guanga, G. P., Les, J. T., and Bourret, R. B. (2001) Alteration of a nonconserved active site residue in the chemotaxis response regulator CheY affects phosphorylation and interaction with CheZ. *J. Biol. Chem.* 276, 18478–18484.